LBL-26941
Preprint

Lawrence Berkeley Laboratory
UNIVERSITY OF CALIFORNIA

Submitted to Nuclear Physics B

Analytic Approximations for Inside-Outside Interferometry

S.S. Padula and M. Gyulassy

November 1989

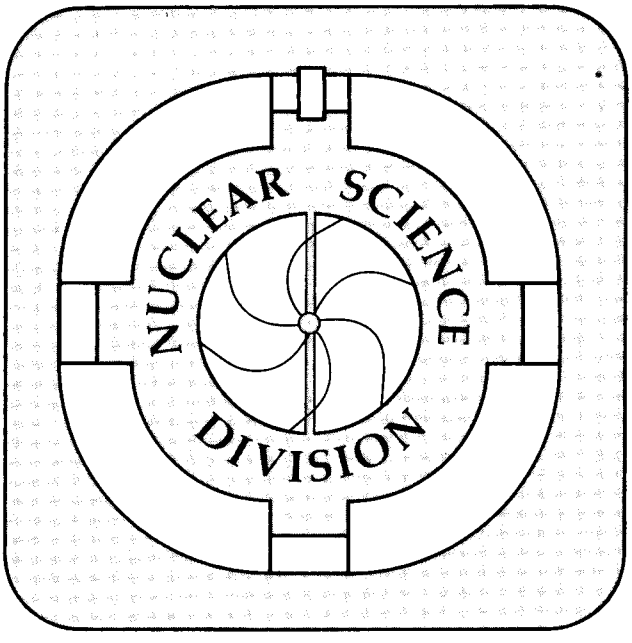

Prepared for the U.S. Department of Energy under Contract Number DE-AC03-76SF00098.

DISCLAIMER

LBL-26941

Analytic Approximations for Inside–Outside Interferometry*

Sandra S. Padula[1] and Miklos Gyulassy

Nuclear Science Division
Mailstop 70A-3307
Lawrence Berkeley Lab
Berkeley, CA 94720 USA

November 3, 1989

Abstract:
Analytical expressions for pion interferometry are derived illustrating the competing effects of various non-ideal aspects of inside-outside cascade dynamics at energies $\sim$ 200 AGeV.

1 Introduction and Summary

Pion interferometry[1]-[7], the pion analogue of Hanbury Brown - Twiss interferometry, is a powerful tool to probe the space-time geometry of hadronic sources. In the case of static sources, e.g. stars, the interferometric pattern depends only on the geometry of the source. However, as stressed in many papers[8,9,12,13,14,15], the interpretation of the interference pattern in high energy reactions depends also on the dynamics. The main reason for this is that strong correlations between momentum and space-time coordinates are expected in that case. In Ref.[13,14] we discussed some of the major effects that could contribute to alter the behavior of the correlation function. We discuss them in more detail here and derive approximate analytical expressions to clarify the competing effects that distort the interference pattern. We present numerical results to illustrate those effects. Our derivation employs the current ensemble formalism[5,11]. As discussed in Ref.[15], this is equivalent to the Wigner density formalism applied to interferometry, in the case of minimum wave packets.

*This work was supported by the Director, Office of Energy Research, Division of Nuclear Physics of the Office of High Energy and Nuclear Physics of the U.S. Department of Energy under Contract No. DE-AC03-76SF00098.

1. Supported by Conselho Nacional de Desenvolvimento Científico e Tecnológico (CNPq), Brazil

The outline of this paper is as follows. In section 2 we recall the equations of the current ensemble formalism[5,11], the correspondent correlation function and the changes introduced by the inclusion of resonances. In section 3 we exhibit the correlation function in the case of the ideal dynamical situation, i.e., the one represented by the so-called inside-outside[16] cascade picture. This corresponds to an uniform rapidity distribution with a fixed proper time geometry and with a delta function correlation between space-time and momentum variables. The approximate analytical form of this correlation function is discussed in the limit of small momentum differences. From this analysis the order of the rapidity scale correlation as well as the increase in transverse radius can be inferred. In this section we also discuss the influence of experimental cuts, like the longitudinal component of the momentum difference (q_L)[12,15] and the rapidity interval on the intercept of the correlation function. The effective intercept of the projected correlation function is shown to be very sensitive to such experimental cuts. In section 4, we study the influence of non-ideal aspects of the dynamics on interferometry. We show that the spread of the freezeout proper time and the non-uniformity of the rapidity distribution go in opposite direction as the spread of the space-time rapidity (η) around the rapidity y. Together, these effects tend to cancel one another. The most significant modification is shown to be the effect due to long lived resonances[17]. Resonances cause the intercept to drop dramatically, as shown in Ref.[13,14]. Finally, in section 5 we present numerical results which illustrate the effects on the correlation function expected from the approximate analytical studies.

2 Ideal Inside–Outside Interferometry

We recall that in the covariant current ensemble formalism[5,11] the pion source is represented by a large ensemble of current elements, each of which is described by

$$j(k) = \sum_a j_0(u_a^\mu k_\mu) e^{ik_\mu x_a^\mu} e^{i\phi_a} \quad , \tag{1}$$

where u_a^μ is the boost velocity of the emitting source and x_a is the space-time origin of current element a; $j_0(x)$ refers to each current element in its rest frame. The factors $e^{i\phi_a}$ are random phases in the case of completely chaotic sources. The inclusive distribution function for n-pions is then given by

$$P_n(k_1, ..., k_n) = \langle \prod_{i=1}^{n} \mid j(k_i) \mid^2 \rangle \quad , \tag{2}$$

where $\langle \cdots \rangle$ denotes the ensemble average over the space-time coordinates x_a, four-velocities u_a, and random phases ϕ_a. In the absence of dynamical multi-pion correlations, that ensemble average can be expressed in terms of the distribution of "freeze-out" phase-space coordinates,

$$D(x,p) = \langle \delta^4(x - x_a) \delta^4(p - p_a) \rangle \quad , \tag{3}$$

where $p_a^\mu = mu_a^\mu$. The n-pion inclusive distribution function is then given by

$$P_n(k_1, ..., k_n) = \sum_\sigma \prod_{i=1}^{n} G(k_i, k_{\sigma_i}) \ , \tag{4}$$

where $\sigma = (\sigma_1, ..., \sigma_n)$ runs over the $n!$ permutations of indices. For the two pion interferometry the complex amplitude $G(k_1, k_2)$ is given by the convolution of the freeze-out distribution and two currents j_0 that contain information about the production dynamics,

$$G(k_1, k_2) = \int d^4p D(q,p) j_0^*(pk_1/m) j_0(pk_2/m) = \langle e^{iqx_a} j_0^*(p_a k_1/m) j_0(p_a k_2/m) \rangle \ , \tag{5}$$

where $q = k_1 - k_2$ is the momentum difference of the two emitted particles.

The two-particle correlation function is then given by

$$C(k_1, k_2) = 1 + \frac{|G(k_1, k_2)|^2}{G(k_1, k_1) G(k_2, k_2)} \ . \tag{6}$$

The model dependence enters through the parameterization of the freeze-out phase-space distribution, $D(x,p)$, and through the model adopted for j_0. In this formalism, the current elements play analogous role as wavepackets do in the Wigner density formalism described in Ref.[15]. We take the covariant pseudo-thermal parameterization as in Ref.[11,13,14], for on shell Fourier transform of the current elements,

$$j_0(pk/m) = e^{-p^\mu k_\mu/(2mT)} \ , \tag{7}$$

for which

$$G(k_1, k_2) = \langle e^{iqx_{af}} e^{-Kp_{af}/(mT)} \rangle \ , \tag{8}$$

where $K = \frac{1}{2}(k_1 + k_2)$.

The effects of long lived resonances can be included in the semiclassical approximation[13,14]. The pion freeze-out coordinates, x_a^μ, can be related to the parent resonance production coordinates, x_r^μ, through

$$x_a^\mu = x_r^\mu + u_r^\mu \tau \ , \tag{9}$$

where u_r^μ is the resonance four velocity and τ is the proper time of its decay. Summing over resonances r of widths Γ_r, and averaging over their decay proper times, we obtain the final expression[13,14]

$$G(k_1, k_2) \approx \langle \sum_r f_{\pi^-/r} \, (1 - iqu_r/\Gamma_r)^{-1} \exp(iqx_r - Ku_r/T_r) \rangle \ , \tag{10}$$

where $f_{\pi^-/r}$ is the fraction of the observed π^-'s arising from the decay of a resonance of type r, and T_r characterizes the decay distribution of that resonance.

3 Ideal Inside-Outside Dynamics

At ultra-relativistic energies the phase space distribution is expected to be longitudinally boost invariant. The most general form in this case is

$$D(x,p) = D(\tau, \eta - y, \mathbf{x}_\perp, \mathbf{p}_\perp)\delta(p_0 - E_p) \ , \tag{11}$$

where $\tau = \sqrt{t^2 - z^2}$, $\eta = \frac{1}{2}\log((t+z)/(t-z))$, $y = \frac{1}{2}\log((E+p_z)/(E-p_z))$ and $\mathbf{x}_\perp$,$\mathbf{p}_\perp$ are the transverse coordinate and momentum. Note that $D(x,p)$ can only depend on the difference between η and y . The ideal inside-outside phase space distribution involves a fixed freezeout proper time τ_f and a perfect correlation between η and y. The correspondent phase-space distribution is written as

$$D(x,p) = \frac{1}{E_f}\rho\frac{1}{\tau_f}\delta(\tau_f - \tau)\delta(\eta - y)\delta(p_0 - E_{\mathbf{p}})g(\mathbf{p}_\perp)\frac{e^{-x_\perp^2/R_T^2}}{\pi R_T^2} \ , \tag{12}$$

where $E_{\mathbf{p}} = \sqrt{\mathbf{p}^2 + m^2}$ is the energy and $g(\mathbf{p}_\perp)$ is the transverse momentum distribution; the rapidity distribution is considered uniform, i.e., $\frac{dN}{dy} = \rho$. To obtain simple analytical equations, we assume a very narrow distribution of $\mathbf{p}_\perp$ around small momenta, i.e., $g(\mathbf{p}_\perp) = \delta^2(\mathbf{p}_\perp)$. The finite pion wavepackets generate the finite $p_\perp$ distribution in our case.

By substituting $D(x,p)$ from (12) into (5) and considering the pseudo-thermal parameterization (7) for the currents, the function $G(k_1,k_2)$ was found to be[11]

$$G(k_1,k_2) = 2\rho e^{-q_T^2 R_T^2/4}K_0(z) \ , \tag{13}$$

where

$$z^2 = [\frac{1}{2T}(m_{1\perp} + m_{2\perp}) - i\tau(m_{1\perp} - m_{2\perp})]^2 + 2(\frac{1}{4T^2} + \tau^2)m_{1\perp}m_{2\perp}[\cosh(\Delta y) - 1] \tag{14}$$

and $\Delta y = y_1 - y_2$.

We are interested here in deriving approximate analytical expressions for the correlation function in suitable kinematic windows in order to clarify the effects of the underlying phase-space distribution of the particles. Consider the approximate form of eq.(13) for small $q = k_1 - k_2$ corresponding to both small q_T and Δy. In that limit,

$$\begin{aligned} m_{1\perp} - m_{2\perp} &\approx \frac{\mathbf{K}_\perp \cdot \mathbf{q}_T}{M_\perp} \ , \\ m_{1\perp} + m_{2\perp} &\approx 2M_\perp \ , \\ m_{1\perp} \cdot m_{2\perp} &\approx M_\perp^2 \ . \end{aligned} \tag{15}$$

Then, making the assumption that

$$\tau_f T \gg \tfrac{1}{2} \ ; \ M_\perp/T \gg \tfrac{1}{2} \ , \tag{16}$$

the argument of the Bessel function in (13) can be approximated by

$$z \approx \frac{M_\perp}{T}[1 - iT\tau\frac{\mathbf{K}_\perp.\mathbf{q}_\perp}{M_\perp^2} + \tfrac{1}{2}T^2\tau^2\Delta y^2] \ . \tag{17}$$

Using the asymptotic expansion of $K_0(z)$, valid for $|z| \gg 1$, i.e.,

$$K_0(z) \approx (\frac{\pi}{2z})^{\frac{1}{2}}e^{-z} \ , \tag{18}$$

we therefore obtain for $G(k_1, k_2)$,

$$G(k_1,k_2) \propto \rho\sqrt{\frac{2\pi T}{M_\perp}}e^{-\mathbf{q}_T^2R_T^2/4}e^{-\frac{M_\perp}{T}[1+\frac{1}{2}T^2\tau^2\Delta y^2]}[1 - \frac{1}{4}T^2\tau^2(\frac{\mathbf{K}_\perp\cdot\mathbf{q}_T}{M_\perp^2})^2] \ . \tag{19}$$

The single particle distribution function is thus given by

$$G(k,k) = 2\rho K_0(\frac{m_\perp}{T}) \approx \rho\sqrt{\frac{2\pi T}{m_\perp}}e^{-\frac{m_\perp}{T}} \ . \tag{20}$$

Note that all the finite spread of transverse momenta follows here from the form of the source current elements and not from their relative motion. Finally, the correlation function for the covariant current ensemble formalism , defined in (6), is given by

$$C(k_1,k_2) \approx 1 + e^{-\mathbf{q}_T^2R_T^2/2}e^{-\frac{1}{4}T^2\tau^2\langle K_\perp^2/M_\perp^4\rangle q_T^2}e^{-M_\perp T\tau^2\Delta y^2} \ , \tag{21}$$

which is then the form of $C(k_1, k_2)$ as function of Δy and q_T in the limit of very small values of these variables. Note that we have averaged over $\mathbf{K}_\perp$ and the angle (ϕ) between the directions of this vector and $\mathbf{q}_T$.

From (21) follows that the rapidity correlation scale is given by

$$\delta y \sim (\bar{p}_\perp\tau_f)^{-1} \quad ; \quad \bar{p}_\perp^2 = \langle M_\perp T\rangle \ . \tag{22}$$

In the limit of $\Delta y = 0$, we see that the effective transverse radius,

$$R_{eff}^2 = R_T^2 + \tfrac{1}{2}T^2\tau^2\langle\frac{K_\perp^2}{M_\perp^4}\rangle \ , \tag{23}$$

is bigger than the real radius, due to the correlation between $K_\perp$ and q_T. This is one of the symptoms of breakdown of the naive interferometric picture, as discussed in [15].

With eq.(21) we can estimate the effective intercept of the correlation function resulting from experimental cuts. That intercept is often misidentified as evidence for coherence and thus it is important to show its kinematic origin[12,15].

Averaging over these kinematical cuts, we obtain

$$\begin{aligned}\langle|G(k_1,k_2)|^2\rangle &\approx \int_{-\infty}^{+\infty}dy_1\int_{-\infty}^{+\infty}dy_2\ \theta[q_{L_b} - |M_\perp\Delta y\cosh(y) + \frac{\mathbf{K}_\perp\cdot\mathbf{q}_T}{M_\perp}\sinh(y)|] \\ &\qquad \theta[Y_{EP} - |y_1|]\quad \theta[Y_{EP} - |y_2|]\quad |G(k_1,k_2)|^2 \\ &\approx \int_{-Y_{EP}}^{+Y_{EP}}dy\int_{\Delta y_1}^{\Delta y_2}d\Delta y\frac{2\pi T}{M_\perp}\,\rho^2\ e^{-\mathbf{q}_T^2R_{eff}^2/2}\ e^{-\frac{2M_\perp}{T}[1+\frac{1}{2}T^2\tau^2\Delta y^2]} \ , \end{aligned} \tag{24}$$

where q_{L_b} is the upper bound on longitudinal momenta cut and $|Y_{EP}|$ delimits the experimental rapidity cut; $y = \frac{1}{2}(y_1 + y_2)$, $\Delta y = y_1 - y_2$ and

$$\begin{aligned} \Delta y_1 &= \frac{-1}{M_\perp \cosh(y)}[q_{L_b} + \frac{\mathbf{K}_\perp \cdot \mathbf{q}_T}{M_\perp}\sinh(y)] \\ \Delta y_2 &= \frac{1}{M_\perp \cosh(y)}[q_{L_b} - \frac{\mathbf{K}_\perp \cdot \mathbf{q}_T}{M_\perp}\sinh(y)] \ . \end{aligned} \tag{25}$$

After integration within the above limits, eq.(24) results in

$$\begin{aligned} \langle |G(k_1,k_2)|^2 \rangle \approx\ & 8\pi \frac{T q_{L_b}}{M_\perp^2}\rho^2 e^{-\frac{2M_\perp}{T}} \arctan[\sinh(Y_{EP})] e^{-\mathbf{q}_T^2 R_{eff}^2/2} \\ & \{1 - \frac{T}{6M_\perp}\tau^2 q_{L_b}^2 [1 + \frac{\sinh(Y_{EP})}{\arctan[\sinh(Y_{EP})]\cosh^2(Y_{EP})}] \\ & - \frac{T\tau^2}{2M_\perp}(\frac{\mathbf{K}_\perp \cdot \mathbf{q}_T}{M_\perp})^2 [1 - \frac{\sinh(Y_{EP})}{\arctan[\sinh(Y_{EP})]\cosh^2(Y_{EP})}]\} \ . \end{aligned} \tag{26}$$

The same integrations performed on $G(k_1,k_1)G(k_2,k_2)$ from eq.(20) gives

$$\langle G(k_1,k_1)G(k_2,k_2)\rangle \approx 8\pi \frac{T q_{L_b}}{M_\perp^2}\rho^2 e^{-\frac{2M_\perp}{T}} \arctan[\sinh(Y_{EP})] \ . \tag{27}$$

The resulting correlation function is

$$\begin{aligned} C(k_1,k_2) \approx\ & 1 + e^{-\mathbf{q}_T^2 R_{eff}^2/2}\{1 - \frac{T}{6M_\perp}\tau^2 q_{L_b}^2 [1 + \frac{\sinh(Y_{EP})}{\arctan[\sinh(Y_{EP})]\cosh^2(Y_{EP})}]\} \\ & \{1 - \frac{T\tau^2}{2M_\perp}(\frac{\mathbf{K}_\perp \cdot \mathbf{q}_T}{M_\perp})^2 [1 - \frac{\sinh(Y_{EP})}{\arctan[\sinh(Y_{EP})]\cosh^2(Y_{EP})}]\} \ , \end{aligned} \tag{28}$$

where we have rewritten the term in between curl brackets into a product, making use of the assumptions $\frac{M_\perp}{T} \gg 1$ and $\frac{|\mathbf{q}_T|}{M_\perp} \ll 1$.

As can be seen from (28) the finite experimental q_L binning lowers the intercept of the transverse projected $C(q_T)$ as a function of q_T. Defining the effective intercept as $C(q_T = 0) = 1 + \lambda_{eff}$, the effective incoherence parameter is seen to be

$$\lambda_{eff} = \{1 - \frac{T}{6M_\perp}\tau^2 q_{L_b}^2 [1 + \frac{\sinh(Y_{EP})}{\arctan[\sinh(Y_{EP})]\cosh^2(Y_{EP})}]\} \ . \tag{29}$$

The other factor that contributes to the decrease of the intercept is given by the term in brackets in eq.(29), which goes to one for large values of Y_{EP} and goes to two for $Y_{EP} = 0$, introducing an unexpected dependence on the experimental rapidity interval. For example, for $\tau = 4$ fm/c, $T = 0.17$ GeV, $q_{L_b} = 0.1$ GeV/c, $Y_{EP} = 1.0$, $K_\perp^2 \approx 0.026$ GeV^2/c^2 and $M_\perp^2 \approx 0.045$ GeV^2, $\lambda_{eff} \approx 0.14$. This shows that, for the cuts typically used in experiments, the intercept is very strongly affected by both finite q_L and Y_{EP}.

4 Non–Ideal Effects

We consider next the effects of relaxing the assumption on uniform rapidity and delta function for the τ and $(\eta - y)$ distributions by modifying the source distribution as in [13,14]

$$\rho \frac{1}{\tau_f}\delta(\tau_f - \tau)\delta(\eta - y) \quad \longrightarrow \quad \frac{2}{\Delta\tau^2} e^{-\tau_f^2/\Delta\tau^2} \; e^{-\frac{(y-y^*)^2}{2Y_c^2}} \; \frac{e^{-\frac{(\eta-y)^2}{2\Delta\eta^2}}}{\sqrt{2\pi}\Delta\eta} \; . \tag{30}$$

In what follows, we consider the case $\mathbf{q_T} = 0$ ($M_\perp = m_{1\perp} = m_{2\perp} = m_\perp$). In this case, $q_L \approx m_\perp \Delta y$ for small differences $\Delta y = y_1 - y_2$ in rapidity.

In order to better discuss the effects of the non-ideal dynamics, we start with the spread in the freezeout proper time and progressively introduce the other effects. Within the same approximations (15,16) of the previous section, we get

$$G(k_1, k_2) \approx \rho \sqrt{\frac{2\pi T}{m_\perp}} \frac{e^{-\frac{m_\perp}{T}}}{[1 + \frac{1}{2} m_\perp T \Delta\tau^2 \Delta y^2]} \; , \tag{31}$$

and $G(k,k)$ is given in (20) above. The correlation function is then

$$C(k_1, k_2) \approx 1 + \frac{1}{[1 + \frac{1}{2} m_\perp T \Delta\tau^2 \Delta y^2]^2} \; . \tag{32}$$

If we compare (21) with (32), we see that the spread in τ converts the exponential into a power law. As a consequence, the correlation function becomes broader.This information is useful when looking into the intercept of the correlation function versus q_T. Of course, any non-zero value of Δy would result into an intercept smaller than 2 [12,15], although this fact has never been taken into account in the experimental analyses and is frequently misinterpreted as a chaoticity parameter smaller than 1. If we then use the result in eq.(32) and fix a value of $\Delta y \ll 1$, we conclude that the spread in time makes the intercept rise.

Next, consider the effect of a non-uniform rapidity distribution. For O+Au at 200 AGeV[10], for example, $Y_c \approx 1.4$ is the rapidity width and $y^* \approx 2.5$ is the CM rapidity. Considering for simplicity that $\frac{1}{2}(y_1 + y_2) \equiv y^*$, the two particle amplitude is then given by

$$G(k_1, k_2) \approx \rho \frac{\sqrt{2\pi}}{\sqrt{\frac{1}{Y_c^2} + \frac{m_\perp}{T}}} \frac{e^{-\frac{m_\perp}{T}}}{[1 + \frac{1}{2} \frac{m_\perp^2 \Delta\tau^2 \Delta y^2}{(\frac{1}{Y_c^2} + \frac{m_\perp}{T})}]} \; , \tag{33}$$

and the single particle distribution is given by

$$G(k,k) \approx \rho \frac{\sqrt{2\pi}}{\sqrt{\frac{1}{Y_c^2} + \frac{m_\perp}{T}}} e^{-\frac{m_\perp}{T}} \; . \tag{34}$$

The resulting correlation function is then

$$C(k_1,k_2) \approx 1 + \frac{1}{[1+\frac{1}{2}\frac{m_\perp^2 \Delta\tau^2 \Delta y^2}{(\frac{1}{Y_c^2}+\frac{m_\perp}{T})}]^2} \ . \tag{35}$$

We see from (35) that we recover (32) in the limit $Y_c \to \infty$. Finite Y_c has then the effect of reducing the denominator in (35), making the correlation function drop even more slowly. As a consequence, for the same fixed values of $\Delta y \ll 1$ and of the other parameters, $C(k_1,k_2)$ becomes broader and even higher than in eq.(32).

The next effect in eq.(30) is the one related to $(\Delta\eta)$, which specifies the rms fluctuations of the space-time rapidity η around the rapidity y. According to the ATTILA version of the LUND Fritiof multi-string model [13,14,18], $\Delta\eta \approx 0.8$. Within the same approximations as in the previous cases, we get, in the CM frame $(y^* = 0)$,

$$G(k_1,k_2) \approx \rho \frac{\sqrt{2\pi}}{\sqrt{\frac{1}{Y_c^2}+\frac{m_\perp}{T}}} \frac{e^{-\frac{m_\perp}{T}}}{[1+\frac{1}{2}m_\perp^2 \Delta\tau^2 \Delta y^2 (\Delta\eta^2 + \frac{1}{\frac{1}{Y_c^2}+\frac{m_\perp}{T}})]} \ , \tag{36}$$

and $G(k,k)$ is the same as in (34). As a result, we obtain for the correlation function

$$C(k_1,k_2) \approx 1 + \frac{1}{[1+\frac{1}{2}m_\perp^2 \Delta\tau^2 \Delta y^2 (\Delta\eta^2 + \frac{1}{\frac{1}{Y_c^2}+\frac{m_\perp}{T}})]^2} \ . \tag{37}$$

The effect of $\Delta\eta$,however, goes in opposite direction as the previous ones: the denominator is increased for finite values of this variable. This makes the correlation function drop faster than before. Consequently, $C(k_1,k_2)$ becomes narrower and the intercept has the tendency of go down, for fixed $\Delta y \ll 1$. In summary, the fluctuations of η around y tend to oppose the two previous effects. Thus, to a large extent, the non-ideal effects tend to cancel one another and the simple formula for the ideal IOC provides a reasonable approximation.

By far the most important non-ideal effect that modifies the form of the correlation function is the influence of long lived resonances. Since the effects of introducing $\Delta\tau$, Y_c and $\Delta\eta$ tend to cancel one another, we treat resonances in the ideal IOC case only.

As we saw in section 2, the inclusion of resonances results in the form for $G(k_1,k_2)$ given in (10). Once more considering the same approximations as before, i.e., for $\mathbf{q}_T = 0$ and $\Delta y = y_1 - y_2 \ll 1$, the two-particle interference amplitude, for the case where all $T_r = T$, can be written as

$$G(k_1,k_2) \approx \rho \sqrt{\frac{2\pi T}{m_\perp}} e^{-\frac{m_\perp}{T}} \sum_r f_r \exp\{-\frac{1}{2} m_\perp T \Delta y^2 (\tau_0 + \frac{1}{\Gamma_r})^2\} \ , \tag{38}$$

where we have exponentiated $(1 - iqu/\Gamma) \approx e^{-iqu/\Gamma}$. For the single-inclusive, since $\sum_r f_r = 1$, we again have the same form as in (20).

In this case, the correlation function can be written as

$$C(k_1,k_2) \approx 1 + \{\sum_r f_r \exp[-\frac{1}{2} m_\perp T \Delta y^2 (\tau_0 + \frac{1}{\Gamma_r})^2]\}^2 \ . \tag{39}$$

Note that resonances lead to the following rapidity correlation scale

$$\delta y \approx [\bar{p}_\perp (\tau_0 + \frac{1}{\Gamma_r})]^{-1} \ , \tag{40}$$

which is the generalization we expect from (22).

Finally, we illustrate by means of simplified analytic equations the effect of smearing in proper time on the transverse radius. As shown in Ref.[15], for the case of a Gaussian source in phase space, time fluctuations may increase the apparent transverse radius. For discussing this, we consider $\Delta y = 0$ and a proper time distribution slightly different than the one in eq.(30). Consider $f(\tau) = \frac{1}{\sqrt{2\pi}\Delta\tau} e^{-(\tau-\tau_0)^2/2\Delta\tau^2}$ for the sake of simplicity. In this case, we get

$$\begin{aligned} G(k_1,k_2) \ \approx \ & \rho \sqrt{\frac{2\pi T}{M_\perp}} e^{-\frac{1}{4} q_T^2 R_T^2} e^{-\frac{M_\perp}{T}} \{1 + i(\frac{\mathbf{K}_\perp \cdot \mathbf{q}_T}{M_\perp})(1 + \frac{T}{2M_\perp})\langle\tau\rangle - \\ & \frac{1}{2}(\frac{\mathbf{K}_\perp \cdot \mathbf{q}_T}{M_\perp})^2 [(1 + \frac{T}{2M_\perp})^2 + \frac{T^2}{2M_\perp^2}]\langle\tau^2\rangle\} \ . \end{aligned} \tag{41}$$

The single particle distribution comes from (20). As a result, the $C(k_1,k_2)$ as a function of q_T is given by

$$C(k_1,k_2) \approx 1 + \exp\{-\frac{1}{2}[R_T^2 + \tfrac{1}{2}T^2\langle\tau^2\rangle\langle\frac{K_\perp^2}{M_\perp^4}\rangle + \Delta\tau^2\langle\frac{K_\perp^2}{M_\perp^2}\rangle] q_T^2\} \ . \tag{42}$$

In comparing (21) with (42) we can clearly notice that the fluctuations in proper-time increases the transverse radius due to the extra term proportional to the width ($\Delta\tau$) of the proper time distribution . We should also notice that the rms in eq.(42) reduces to $\langle\tau^2\rangle^{\frac{1}{2}} = \tau_0$ for the case of delta function distribution in proper-times given by (21).

To summarize, if we add all the effects discussed above, we notice that the non-ideal IOC picture plus resonances can be one possible explanation for apparent large radius (narrow correlation function) and small intercept observed experimentally and reported in Ref.[10].

5 Numerical Results

Due to limited statistics, it is in general not possible to compare theoretical correlation functions, $C(\mathbf{q},\mathbf{K})$, depending on the six independent variables with data. Instead one is forced to introduce integrated or "projected" correlation functions depending on fewer variables. In NA35[10], for example, a two dimensional correlation

function was defined as a function of q_L and q_T as follows

$$C_{35}(q_T, q_L) = \frac{\int d\phi_q d^3\mathbf{K}\ \Theta_c(\mathbf{q},\mathbf{K})\ P_2(\mathbf{K}+\frac{1}{2}\mathbf{q}, \mathbf{K}-\frac{1}{2}\mathbf{q})\ A_2(\mathbf{q},\mathbf{K})}{\int d\phi_q d^3\mathbf{K}\ \Theta_c(\mathbf{q},\mathbf{K})\ P_1(\mathbf{K}+\frac{1}{2}\mathbf{q}) P_1(\mathbf{K}-\frac{1}{2}\mathbf{q})\ A_2(\mathbf{q},\mathbf{K})}\ , \qquad (43)$$

where $\Theta_c = 1$ only in a specific kinematic region and $= 0$ outside that region, and A is the experimental acceptance function. For NA35, $\Theta_c = 1$ for pions with a rapidity, y, in a finite interval, $y_1 \leq y \leq y_2$. In (43), ϕ_q is the azimuthal angle of $\mathbf{q}$ with respect to the beam axis. Unfortunately, the measured correlation function also depends on the two pion acceptance function, $A_2(\mathbf{q},\mathbf{K})$, which is generally not known with precision. A rough guess for A_2 can be obtained by assuming $A_2 = A_1(\mathbf{k}_1)A_1(\mathbf{k}_2)$, where A_1 is the single particle efficiency. This assumption however cannot be taken for granted because the efficiency to detect pairs varies small q in general. From the single pion inclusive distribution presented in [10], $A_1(\mathbf{k})$ is maximal at mid rapidity with $A_1 \sim 0.8$ at $y \sim 2.5$ and decreases to ~ 0.5 on both sides at $y \sim 1$ and 4. The final experimental correlation function is a matrix, $C_{35}(i,j)$, involving additional integrations over q_T and q_L over finite bins of width 10 MeV.

We now show numerical results for illustrating the non-ideal effects discussed above within special kinematic windows for each case. The same numerical methods and code were used here as led to the result reported in [13,14]. In Fig.1 we study the case $R_T = 4.0$ fm, $\tau = 4.0$ fm/c and fixed the chaoticity parameter to unity, i.e., $\lambda = 1.0$. For the parameters of the non-ideal dynamics we adopted $\Delta\tau = 4.0$ fm/c, $Y_c \approx 1.4$ and $\Delta\eta \approx 0.8$, where the last two values come from the ATTILA version of the LUND string model[18]. In this figure, the correlation functions versus Δy are shown for each case, starting with the parameterization corresponding to the ideal IOC and adding the non-ideal parameters step by step. We can see that the numerical results follow the behavior of the correlation function anticipated by the simplified analytical equations discussed in section 4: the smearing in proper time makes the correlation function broader, and so does the finite (Gaussian) rapidity distribution; the inclusion of the fluctuations between η and y, on the other hand, pushes into the opposite direction, practically compensating for the first two effects. The inclusion of resonances then narrows $< C(\Delta y) >$ even more. For comparison we exhibit the effect of resonances alone, which really produces the major global effect. We should note that the intercept in this last case is smaller than two because we have considered only the following fractions[13,14] of resonance decaying into pions: $f_{\pi^-/direct} \approx 0.19$, $f_{\pi^-/\rho} \approx 0.40$, $f_{\pi^-/\omega} \approx 0.16$, and $f_{\pi^-/K^*} \approx 0.09$, all others being set to zero.

Next, in Figure 2, we show the results of the correlation function versus q_T when the smearing in proper time is introduced, fixing $\Delta y = 0.0$, $\lambda = 1.0$ and $R_T = 4.0$ fm. Three values of $\Delta\tau^2 =< \tau^2 > - < \tau >^2$ are considered. We see that, for increasing $\Delta\tau$, the correlation function becomes narrower, i.e., the radius increases, as expected from eq.(42). We also include the case with no smearing (ideal IOC), represented by the curve with $\tau_0 = 4.0$ fm.

Finally, in Figure 3, we show numerical results for the correlation function versus q_T, for the same values of the parameters of Figure 1, except that here we consider

a finite interval for q_L (< 0.10 GeV/c). Due to the fact that q_L is not zero, the intercept is smaller than two even for the ideal IOC case[12,15]. We can see that the progressive inclusion of the non-ideal effects result into similar behavior for the correlation function as seen in Figure 1. The curves here are not smooth in order to show that the results are very sensitive to the available statistics. We also include in Figure 3 the experimental data from NA35[10].

Acknowledgements:

One of us (SSP) would like to express her gratitude to the Nuclear Theory Group for the kind hospitality during the development of the present work.

References

[1] R. Hanbury-Brown and R.Q. Twiss, Phil. Mag. 45 (1954) 663; Nature 177 (1956) 27 and 178(1956) 1447.

[2] G. Goldhaber, et al., Phys. Rev. 120 (1960) 300.

[3] G. I. Kopylov, Phys. Lett. 50B (1974) 572.

[4] E.V. Shuryak, Phys. Lett. 44B (1973) 387.

[5] M. Gyulassy, et al., Phys. Rev. C20 (1979) 2267.

[6] W. A. Zajc, et al., Phys. Rev. C29 (1984) 2173.

[7] M. Gyulassy, Phys. Rev. Lett. 48 (1982) 454.

[8] S. Pratt, Phys. Rev. Lett. 53 (1984) 1219.

[9] D. Beavis, et al., Phys. Rev. C27 (1983) 910.

[10] T. J. Humanic, et al. , Z. Phys. C38 (1988) 79;
A. Bamberger, et al. Phys. Lett. B203 (1988) 320.

[11] K. Kolehmainen, M. Gyulassy, Phys. Lett. 180B (1986) 203.

[12] Y. Hama, S. S. Padula, Proceedings of the 2^{nd} International Workshop on Local Equilibrium in Strong Interaction Physics – LESIP II (1986), p. 63, ed. por P. Carruthers e D. Strottman;
Y. Hama, S. S. Padula, Phys. Rev. D37 (1988) 3237.

[13] S. S. Padula and M.Gyulassy, Nucl. Phys. A498 (1989) 555c.

[14] M. Gyulassy, S. S. Padula, Phys. Lett. 217B (1989) 181.

[15] M. Gyulassy, S. S. Padula and S. Gavin, LBL-24647 (1989), Nucl. Phys. B, in press.

[16] J.D. Bjorken, Phys. Rev. D27 (1983) 140.

[17] P. Grassberger, Nucl. Phys. B120 (1987) 231.

[18] B. Andersson, et al., Nucl. Phys. B281 (1987) 289;
M. Gyulassy, CERN-TH.4794 (1987), Proc. Eight Balaton Conf. on Nucl. Phys. (ed. Z. Fodor, KFKI, Budapest 1987).

Figure Captions

Figure 1:
Numerical results for the pion correlation function versus Δy, for $q_T = 0$ and in the central rapidity region. The non-ideal effects are introduced step by step. We also show the dramatic effect of resonances alone on $C(k_1, k_2)$.

Figure 2:
Numerical results for the pion correlation function versus q_T, for $\Delta y = 0$, again in the central region. Here we show that the increase in the with of the (smeared) proper-time distribution makes the correlation function progressively narrower. We illustrate this effect for three values of $\Delta\tau$.

Figure 3:
Similarly to Fig. 1, we show numerical results for $C(k_1, k_2)$ but as a function of q_T, when the non-ideal effects are introduced one by one. We notice that the qualitative behaviour of the present curves are similar to the correspondent ones on Fig. 1 with respect to the general trend of each effect. The rapidity interval of each particle of the pair is the central one ($2 \leq y \leq 3$ for NA35 or $-0.5 \leq y^* \leq 0.5$ in the CM frame).

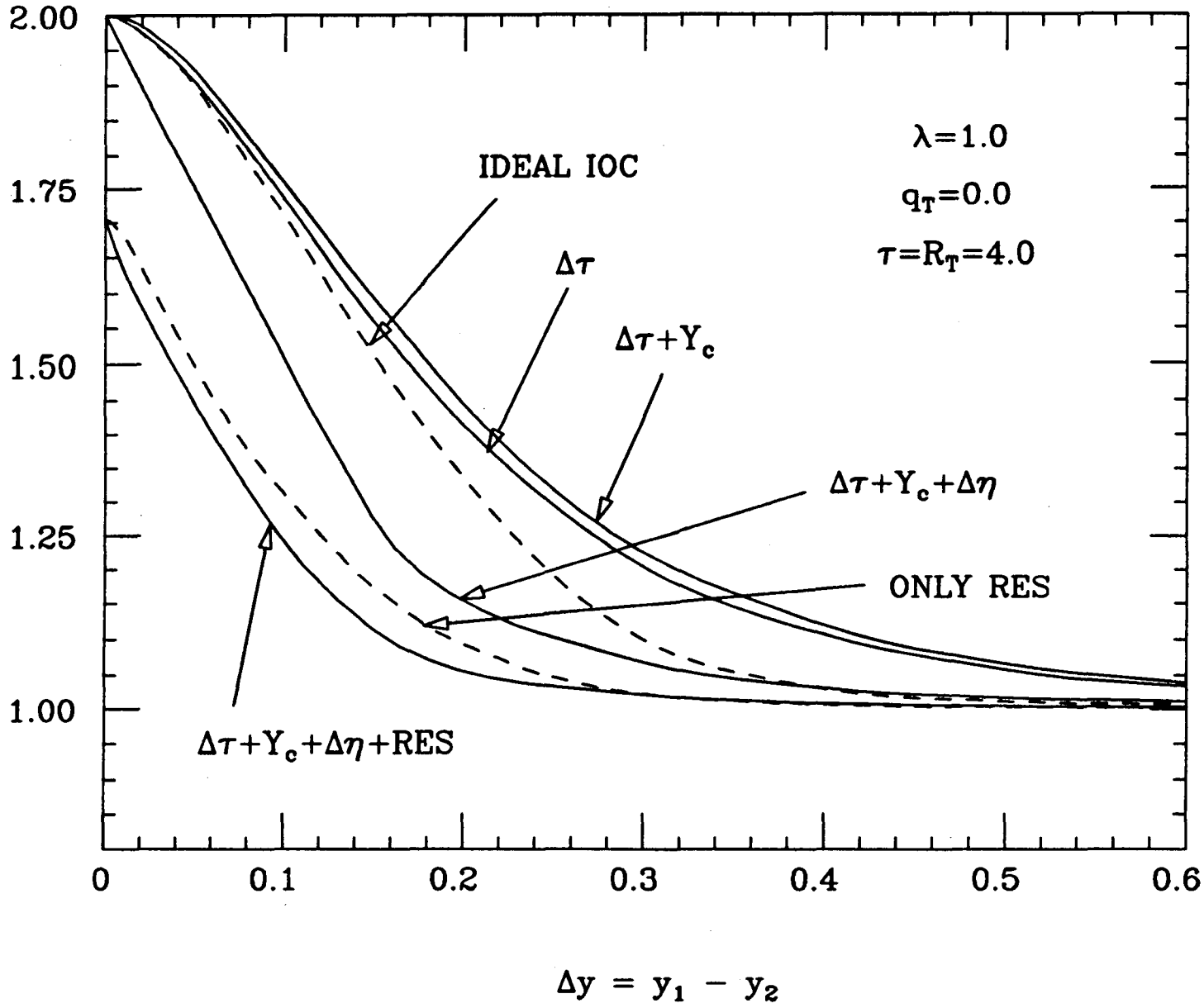
2.00
1.75
1.50
1.25
1.00
0
0.1
0.2
0.3
0.4
0.5
0.6
< C (Δy) >
Δy = y1 − y2
λ=1.0
qT=0.0
τ=RT=4.0
IDEAL IOC
Δτ
Δτ+Yc
Δτ+Yc+Δη
ONLY RES
Δτ+Yc+Δη+RES

Figure 1

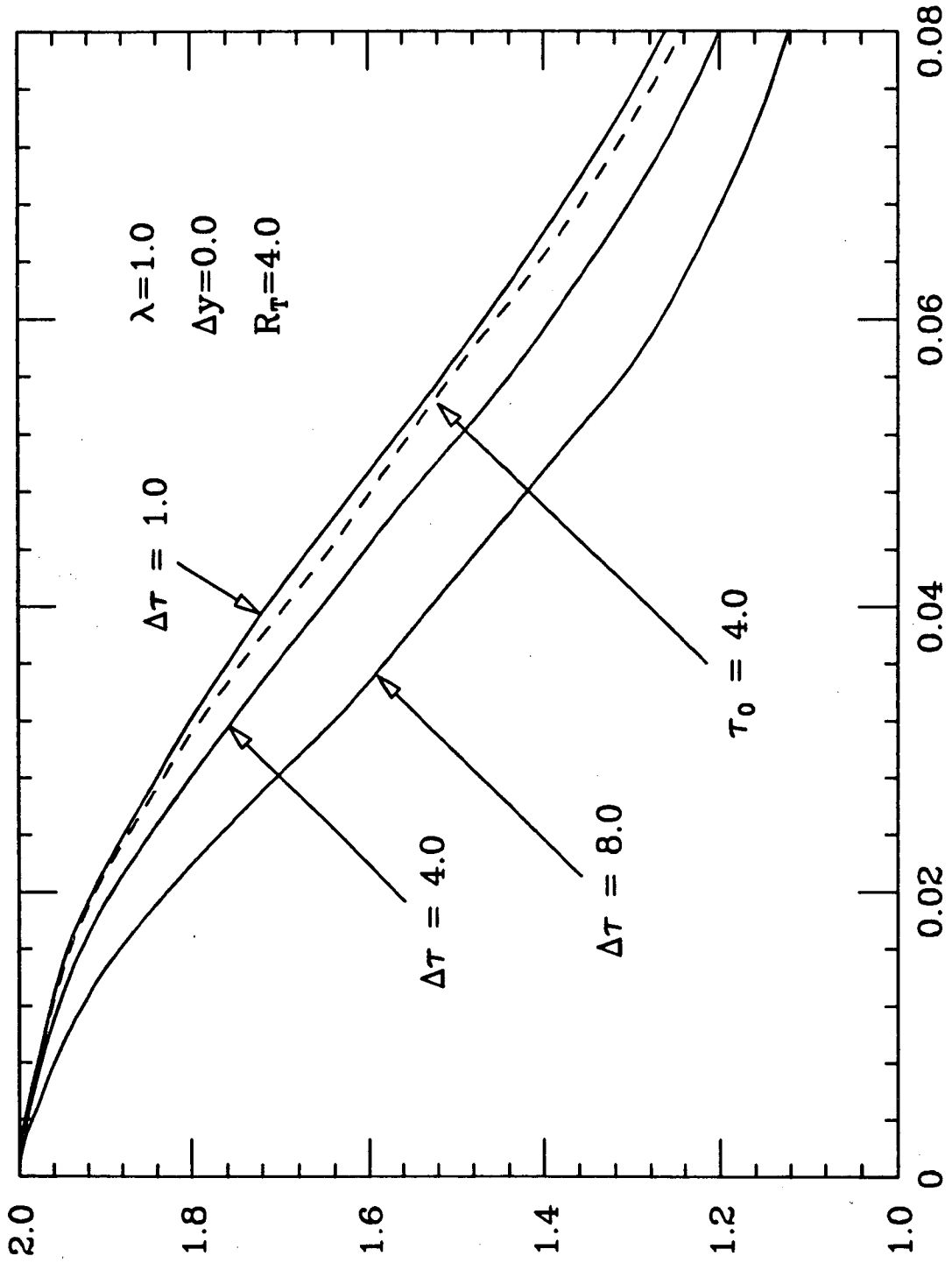
λ=1.0
Δy=0.0
R_T=4.0
Δτ = 1.0
Δτ = 4.0
Δτ = 8.0
τ_0 = 4.0
< C (q_T) >
q_T (GEV)
2.0
1.8
1.6
1.4
1.2
1.0
0
0.02
0.04
0.06
0.08

Figure 2

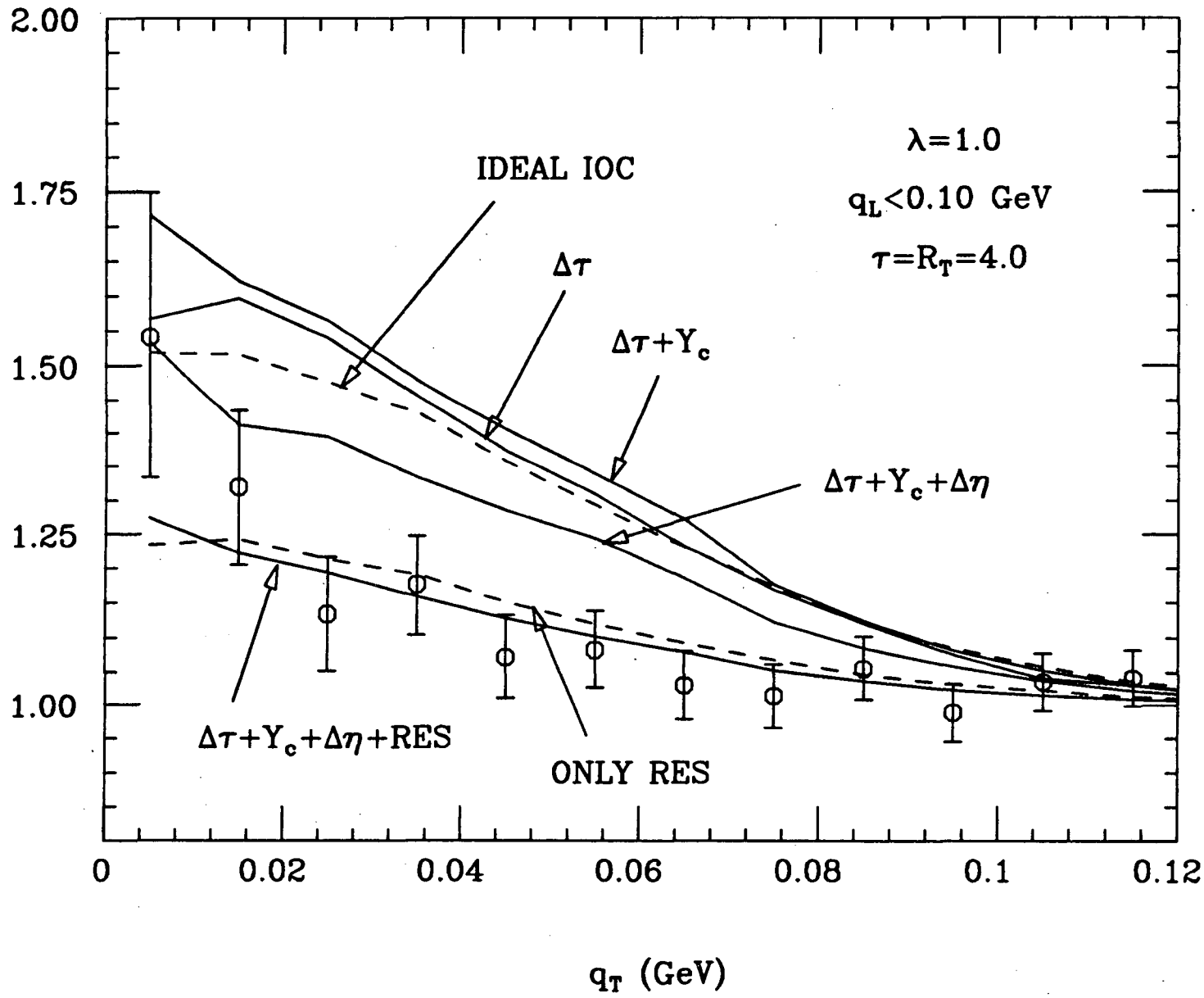
2.00
1.75
1.50
1.25
1.00
< C (q_T) >
0
0.02
0.04
0.06
0.08
0.1
0.12
q_T (GeV)
IDEAL IOC
$\Delta\tau$
$\Delta\tau+Y_c$
$\Delta\tau+Y_c+\Delta\eta$
$\Delta\tau+Y_c+\Delta\eta+RES$
ONLY RES
$\lambda=1.0$
$q_L<0.10$ GeV
$\tau=R_T=4.0$

Figure 3

LAWRENCE BERKELEY LABORATORY
TECHNICAL INFORMATION DEPARTMENT
1 CYCLOTRON ROAD
BERKELEY, CALIFORNIA 94720